Journal of Biological Physics 31: 433–452, 2005.
DOI: 10.1007/s10867-005-0171-2

Protein Surface Dynamics: Interaction with Water and Small Solutes

RAN FRIEDMAN*, ESTHER NACHLIEL and MENACHEM GUTMAN
Laser Laboratory for Fast Reactions in Biology, Department of Biochemistry, The George S. Wise Faculty for Life Sciences, Tel Aviv University, Tel Aviv, Israel
*(*Author for correspondence, e-mail: ran@hemi.tau.ac.il)*

Abstract. Previous time resolved measurements had indicated that protons could propagate on the surface of a protein, or a membrane, by a special mechanism that enhances the shuttle of the proton towards a specific site [1]. It was proposed that a proper location of residues on the surface contributes to the proton shuttling function. In the present study, this notion was further investigated using molecular dynamics, with only the mobile charge replaced by Na^+ and Cl^- ions. A molecular dynamics simulation of a small globular protein (the S6 of the bacterial ribosome) was carried out in the presence of explicit water molecules and four pairs of Na^+ and Cl^- ions. A 10 ns simulation indicated that the ions and the protein's surface were in equilibrium, with rapid passage of the ions between the protein's surface and the bulk. Yet it was noted that, close to some domains, the ions extended their duration near the surface, suggesting that the local electrostatic potential prevented them from diffusing to the bulk. During the time frame in which the ions were detained next to the surface, they could rapidly shuttle between various attractor sites located under the electrostatic umbrella. Statistical analysis of molecular dynamics and electrostatic potential/entropy consideration indicated that the detainment state is an energetic compromise between attractive forces and entropy of dilution. The similarity between the motion of free ions next to a protein and the proton transfer on the protein's surface are discussed.

Key words: molecular dynamics, ions at interface, protein-salt interactions

Introduction

Biological reactions, such as binding of a ligand to its receptor, insertion of an ion into a channel, and protein folding, occur at the interface between a protein and the surrounding solvent. Accordingly, before such a reaction takes place, the surfaces of the reactants must lose some of their solvation shell. Furthermore, the interaction between the protein and the innermost water molecules will modulate the physical-chemical properties of the first solvation shell of the macromolecule. For these reasons, the protein-solvent interface has been excessively studied using various experimental and theoretical methods (reviewed in [2, 3]). The studies described in these reviews, and numerous other studies of the protein-solvent environment [4–9], focused on the hydration pattern of the proteins. However, a complete description

of the protein-solvent interface cannot be accomplished without considering the surface residues and the salt ions, which are an integral part of all physiological systems.

Protein-salt interactions have been studied both experimentally and theoretically. The effects of salt on the stability and solubility of protein (i.e. salting-in and salting-out) have been long known. Furthermore, salt ions were experimentally found to be bound to the surface of the protein lysozyme [10]. Yet, owing to the experimental difficulties in studying the dynamics of ions on protein surfaces on the molecular scale, ligand exchange reactions which involve small ions on the protein surface can only be studied using computer simulations.

Our interest in the protein-water interface stemmed from the kinetic measurements of proton transfer at the surface of proteins [11–21]. A direct method for studying the proton-protein dynamics is based on the Laser Induced Proton Pulse technique [18, 22–24]. In these studies, proteins were dissolved or suspended in a solution containing photoacid (photoacids are molecules whose pK_as are dramatically reduced when excited to their first electronic singlet state [25–28]). The excitation of the photoacid molecules led to a rapid proton release into the solution. Following the momentary acidification of the solution, surface groups such as histidine, aspartate and glutamate became transiently protonated. Using probe molecules attached to the protein, the kinetics of the proton transfer reactions on the protein surface could be analyzed. It was noted in these studies that residues, which according to the crystal structure of the protein are up to 10–15 Å apart, could form proton-attractive domains and share the proton among them at a very fast rate, exceeding the upper limit of diffusion-controlled reactions as characterized by the Debye-Smoluchowski equation [29–31]. To account for the fast rate, it was suggested that the dynamics of the protein generate transient situations in which the residues are getting sufficiently close to allow a proton transfer over a short distance. Furthermore, the passage of the proton is accelerated by the electrostatic potentials that bias the diffusion of the proton between the donor-acceptor sites. It was also reasoned that, if such a mechanism is operative, it should be a general feature of the protein surface and not limited to a specific protein or charged particle. In the present study, we wish to demonstrate that the protein surface has the ability to attract small charged ligands, to hold them near the protein surface, and to shuttle them between surface residues.

In order to test the above hypothesis, we carried out molecular dynamics (MD) simulations of a model protein, studying the various aspects of ion propagation near the surface of the protein. The results of the simulations were analyzed with respect to the detainment of the ions (both Cl^- and Na^+) at the immediate vicinity of the protein. It was found that the probability of finding the ions near the protein was higher than expected due to thermal motions. Additionally, the ions tend to localize near specific attractor domains. From the Brownian motion of the ions, we generalized how protons or small ligands may propagate near the surface of a protein. On the basis of these observations, we can draw out the general features of

surface domains that are instrumental for efficient delivery of solutes to an active site on the protein surface.

The protein, which was selected as a model for this study, is S6, which forms part of the bacterial 30S ribosome central domain [32] and has no function associated with ion transport on its surface. S6 is a globular protein of 101 amino acids, 32 of which are charged at a physiological pH. Moreover, owing to its high charge density and globular structure, all the amino acids are at least partially exposed to the bulk (i.e. no amino acid is totally buried in the protein matrix). In order to be consistent with chemical experiments, which have been undertaken in our lab with the S6 Q16H/S17C double mutant, we have performed our simulations using the same mutant protein.

Methods

Molecular dynamics simulations

The molecular dynamics (MD) simulations were performed using the GROMACS 3.1 package of programs [33], with the GROMACS force field, which is a modified version of the GROMOS87 force field [34–38]. The calculations were carried out using the structure of the S6 ribosomal protein (PDB code 1RIS) determined by Lindahl and co-workers [39], and downloaded from the Protein Data Bank [40]. The starting structure was prepared by replacing the side chains of residues Glu16 and Ser17 with histidine and cysteine, respectively. The protein was embedded in a box containing SPC model water [41] that extended to at least 8 Å between the protein and the edge of the box. Although more complex water models are nowadays frequently used in the simulation of proteins, we chose to use the SPC, as it was found to give superior results for simulations of solutes in water when compared to more sophisticated water models [42], especially at interfaces [43]. The total number of water molecules was 6677. Four Na^+ and four Cl^- ions, corresponding to a salt concentration of $\sim$30 mM, were added to the system in random positions.

Prior to the dynamics simulation, internal constraints were relaxed by energy minimization. Following the minimization, an MD equilibration run was performed under position restraints for 20 picoseconds. A 10 nanoseconds long production MD run was performed after the equilibration. During the MD run, the LINCS algorithm [44] was used in order to constrain the lengths of hydrogen-containing bonds; the waters were restrained using the SETTLE algorithm [45]. The time step for the simulation was 2 femtosecond. The simulations were run under NPT conditions, using Berendsen's coupling algorithm [46] for keeping the temperature and the pressure constant ($P = 1$ bar, $\tau_P = 0.5$ picosecond; $T = 300^\circ$K; $\tau_T = 0.1$ picosecond). VDW forces were treated using a cutoff of 12 Å. Long range electrostatic forces were treated using the particle mesh Ewald method [47]. The coordinates were saved every 0.5 picosecond.

CONTINUUM ELECTROSTATICS

The electrostatic contribution to the binding energies was calculated by Eq. (1):

$$\Delta G_{\mathrm{el}} = \Delta G_{\mathrm{solv,complex}} - \Delta G_{\mathrm{solv,protein}} - \Delta G_{\mathrm{solv,ligand}} + \Delta G_{\mathrm{coul,complex}} - \Delta G_{\mathrm{coul,protein}} \quad (1)$$

where ΔG_{solv} and ΔG_{coul} refer to the Poisson-Boltzmann and pairwise Coulombic energy terms associated with the transfer of the solute from a continuum medium with a low dielectric constant ($\varepsilon = 4$, 10 or 20) to a continuum medium with a dielectric constant of water ($\varepsilon = 78.4$). The calculations were performed using two configurations: one where the protein binds a chloride ion to its most attractive site (see Figure 6A) and the second when a Na^+ ion is located in the vicinity of the carboxylate of Glu31 (see Figure 6B). The calculations were carried out as follows. First, the structure of the protein, the ions and the solvent was extracted from the MD simulation. To make sure that the structure does not contain any unfavorable interactions between the atoms, the system was energy-minimized using GROMACS. Following the minimization, the coordinates of the protein and the ion were used for the calculation of ΔG_{el}. The solvation energies were calculated using APBS [48] with a grid spacing of 0.33 Å. In order to make sure that the calculations were independent of the grid size, the calculations were repeated using a grid spacing of 0.4 Å; this had a marginal effect on ΔG_{el} (the largest difference was 0.42 KJ mol^{-1}). All calculations were carried out by solving the non-linear Poisson-Boltzmann equation for the protein in a solution of 50 mM NaCl.

GRAPHICAL PRESENTATION

A graphical presentation of the electrostatic potential of the protein was calculated using the program APBS [48] with a solute dielectric value $\varepsilon = 2$, a solvent dielectric value $\varepsilon = 78.4$ and a grid spacing of 0.4 Å.

All protein figures were created using the VMD computer program [49].

Results

SIMULATION OF THE PROTEIN DYNAMICS

The stability of the protein during the simulation was evaluated by the root mean square deviation (RMSD) of the protein backbone, using the crystal structure of the wild type protein as a reference. During the initial phase of the simulation, ($\sim$20 picosecond) the protein exercised some relaxation, and after that the backbone RMSD remained stable, exhibiting fluctuations that reached a maximal value of 2.8 Å during the 10 nanosecond simulation.

SIMULATION OF THE WATER IN THE BULK

In order to characterize the overall dynamics of the solvent, the diffusion coefficient of the water was calculated from its mean square displacement. The calculated value, $4.021 \pm 0.089\ 10^{-5}$ cm^2 second^{-1}, is larger than the experimental diffusion coefficient of water ($2.4 \cdot 10^{-5}$ cm^2 second^{-1} at room temperature) and is attributed to the rigidity of the water molecule in the model (SPC). Other simulations of SPC type water [50] have yielded values (4.1–4.3 10^{-5} cm^2 second^{-1}) that are comparable with ours, indicating that the higher diffusion coefficient is a feature of the model and not a flaw of the simulation.

THE DYNAMICS OF THE IONS

The mean square deviation (MSD) of the ions was calculated with respect to their initial (random) placement. The variation of the MSD as a function of simulation time is presented in Figure 1. The diffusion coefficients of the ions, as calculated

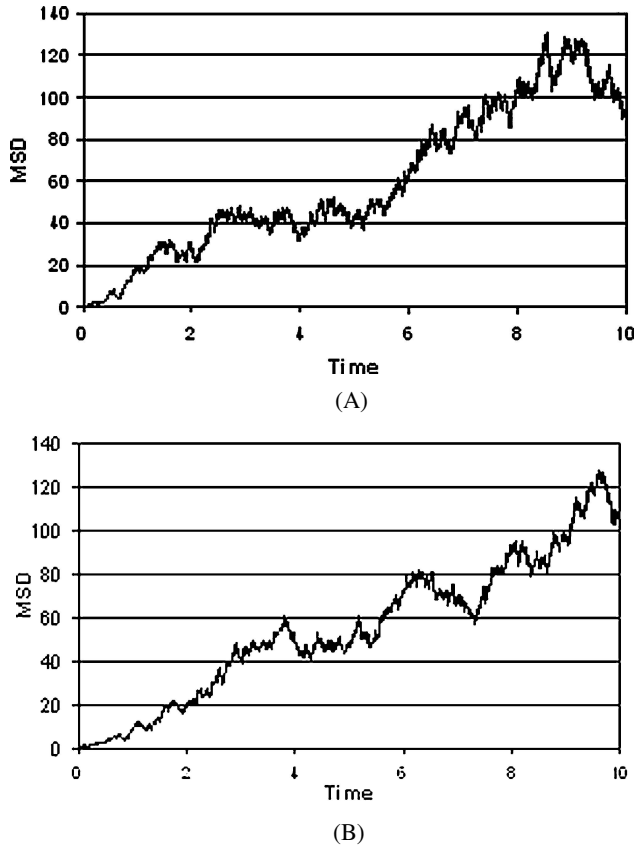

Figure 1. The mean square deviations (MSD) of the Cl^- (Frame A) and Na^+ (Frame B) ions as a function of simulation time. The MSD are given in nm^2 and the time is given in nanoseconds.

from the MSDs, were $1.94 \pm 0.28\ 10^{-5}$ cm^2 second^{-1} and $1.80 \pm 0.19\ 10^{-5}$ cm^2 second^{-1} for the Cl^- and Na^+ ions, respectively. These values are close to the measured diffusion coefficient of dilute NaCl solutions ($\sim 1.5\ 10^{-5}$ cm^2 second^{-1}; see [51, 52]), which is an indication that, despite the simplicity of the water model and the small number of ions, the simulation of the Brownian motion of the ions is realistic.

CONTACTS BETWEEN THE IONS AND THE PROTEIN

The distance between the nearest ions and the protein (minimal distance) during the 10 nanosecond observation time varies from a contact distance $\sim$2 Å up to $\sim$22 Å (Figure 2). Yet the distribution of the minimal distance vs. time is not random; there are distinct states where one of the ions is located close to the

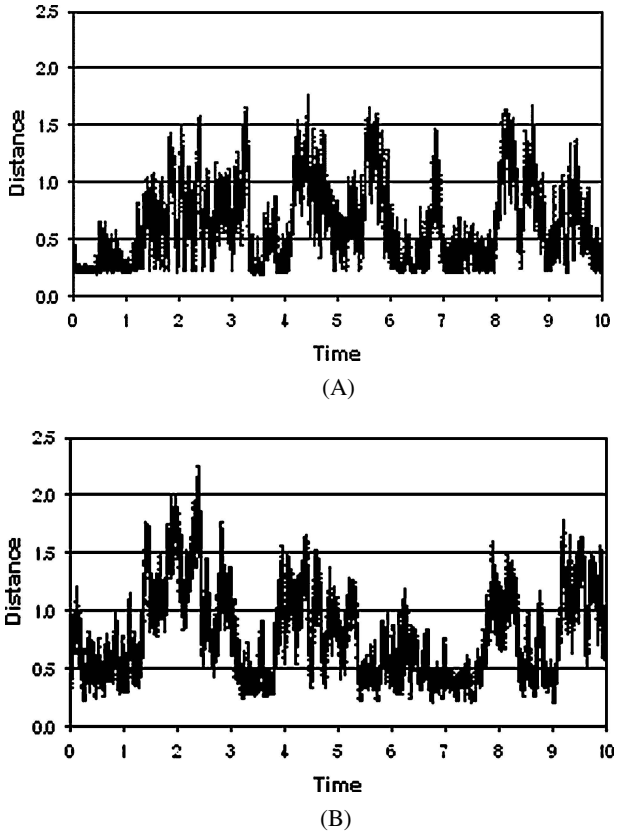

Figure 2. The minimal distance, in nm, between any of the Cl^- (Frame A) and Na^+ (Frame B) ions and the protein as a function of simulation time. The distances are given in nm and the time is given in nanosecnds. The minimal distance is dictated by the steric interferences between the Van der Waals radii of the ions.

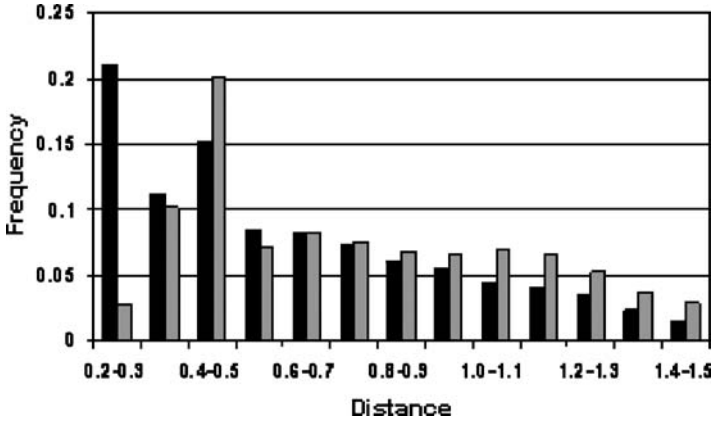

Figure 3. The distribution function for the minimal distances between the Cl^- ions (black) or Na^+ ions (gray) and the protein. The distances are given in nm. Only the main part of the distribution (between $d = 0.2$ nm and $d = 1.5$ nm) is shown.

protein for time frames as long as 1 nanosecond. To evaluate the significance of this time frame, let us consider an ion located at 2 Å distance from an atom on the protein. If this ion's diffusion is a Brownian motion due to thermal fluctuations, the time needed for its diffusion to a distance of 6 Å from the protein would be $\tau \sim 40$ picoseconds (following Einstein's diffusion theory, $\tau = (4\text{Å})^2/2D$). As seen in Figure 2, there are time windows extending up to few hundreds of picoseconds, where the ions seem to remain less than 6 Å away from the protein. When an ion is delayed near the protein for such a time period, its dynamics reveal more than just random thermal fluctuations. Rather, its motion is perturbed by the presence of the protein.

The data presented in Figure 2 were further analyzed by studying the distribution of the minimal distances between the ions and the protein. Figure 3 presents the overall probabilities of finding an ion at a given minimal distance from the protein. It can be seen that for the Cl^- ions, the functions have two maxima (at $d = 0.2$–0.3 nm and at $d = 0.4$–0.5 nm), while for the Na^+ ions there is only one maximum (at $d = 0.4$–0.5 nm). The difference between the ions is ascribed to the nature of the attractor sites on the protein's surface. Electrostatic interactions will favor the closest location of the ion with respect to the attractor site. Still, when an ion is attracted by a single amino acid (for example, see Figure 6B), the electrostatic attraction is counteracted by the entropic tendency of the ion to be dispersed in the bulk, favoring the location of the ion slightly away (4–5 Å) from the protein surface, where it also retains its solvated state. While each of the attractor sites for the sodium is made of one carboxylate moiety, the Cl^- attractor is more complex in nature, consisting of two arginine residues (Arg80, Arg87) and the hydroxyl group of Tyr50 (see Figure 6A below). The ion is partially inserted among these moieties so that when it moves away from one moiety, it gets closer to the others. As only

the closest distance between the ion and the protein is counted, the Cl^- distribution function has a marked maximum at the 2–3 Å interval (Figure 3).

QUANTITATION OF THE ION INTERACTION WITH THE PROTEIN'S SURFACE

The residues on the protein's surface differ in their ion attractiveness. In order to quantitate the affinity of the attractor sites for the ions, we assign an operational definition for the ion affinity. This definition is based on the distribution probability histogram presented in Figure 3. The ions that are located close to the protein surface are defined as *detained*, thus signifying that they are still able to execute a random walk but are under some restrictions that retain them near the surface longer than expected for an unbiased, free-diffusing particle.

In order to quantitate the detainment events, we have used a two-state model where the ion is defined either as *detained* or as *undetained* (free-diffusing) based on a distance criterion. The cutoff distance was defined as 6 Å, based on the characteristic minimal distance between the ions and the protein (4–5 Å, Figure 3), which was stretched by an extra 1 Å (assuming that the ion affinity is not sharply turned off at its maximum).

The mutated protein S6 Q16H/S17C contains 17 positive residues and 17 negative residues (including the C- and N-termini). For each of the charged residues, we calculated the time frame in which an ion was within the 6 Å from its charge-bearing atoms (OD in Asp, OE in Glu, HE or HH in Arg, HZ in lysine, and the C-terminal oxygens or N-terminal hydrogens). The results are summarized in Tables I and

Table I. The frequency of formation of a detained state, where a Cl^- ion is located within 6 Å of the terminal group hydrogens of the N-terminus, Arg or Lys, or the hydrogen from the OH group of Tyr50.

Residue	Frequency	Detainment Energy (KJ/mol)
Met1 (NT)	0.01	2.72
Arg2	0.02	0.96
Arg3	0.004	5.02
Arg28	0.001	8.49
Arg36	0.008	3.28
Tyr50	**0.11**	**−3.51**
Lys54	0.04	−0.82
Arg71	0.007	3.62
Arg80	**0.28**	**−6.40**
Arg87	**0.24**	**−5.88**
Lys92	0.005	4.46

Note. Only residues that are able to detain the ion are presented. The detainment energies were calculated as explained in the text.

Table II. The frequency of formation of a detained state, where a Na^+ ion is located within 6 Å of the carboxylate oxygens of the C-terminus, Asp or Glu and the unprotonated imidazole nitrogen of His16.

Residue	Frequency	Detainment Energy (KJ/mol)
Glu5	0.03	−0.08
Asp15	0.06	−1.89
His16	0.03	−0.08
Glu31	0.07	−2.30
Glu38	0.01	2.72
Glu41	0.08	−2.66
Glu42	0.005	4.46
Glu66	0.005	4.46
Asp70	0.003	5.74
Glu83	0.01	2.72
Glu95	**0.12**	**−3.78**
Phe97 (CT)	0.08	−2.66

Note. Only residues which are able to detain the ion are presented. The detainment energies were calculated as explained in the text.

II. Residues which detain an ion for longer than 10% of the simulation time are highlighted in bold face. Examination of the tables reveals that, of the many ion attractors on the protein surface, most were hardly able to detain an ion. On the other hand, a handful of attractors could detain an ion throughout large fractions (up to 28%) of the simulation times.

The two-state model presented above does not account for the duration of the detainment of the ions. Even if the ion merely approaches within 6 Å of the protein surface by chance, it will be counted as being detained. Yet, such random encounters are so short that their contribution to the overall statistics is negligible: as demonstrated in Tables I and II, there is no difficulty in discriminating between the attractors that keep an ion in their vicinity for an appreciable time and the brief encounters with the less attractive sites.

THE DETAINMENT ENERGY

As demonstrated in Figure 2, there were many encounters between the ions and the protein during the 10 nanosecond simulation. Accordingly, we consider the system as being in equilibrium regarding the detainment of the ions, and use expressions derived from equilibrium thermodynamics to describe the equilibrium detainment dynamics.

The detainment equilibrium constant K_{det} is calculated as [53, 54]:

$$K_{\text{det}} = \alpha/[(1-\alpha)C] \tag{2}$$

where C is the concentration of the ions (0.03 M in the current simulation) and α is the time fraction that the site is associated with an ion, as given in Tables I and II, second column. Accordingly, the energy associated with the detainment is given by the expression

$$\Delta G_{\text{det}} = -RT \ln K_{\text{det}}. \tag{3}$$

The energies, which were calculated for the different residues that detain the ions, are given in the third columns of Tables I and II.

In comparison with the occasional ion-protein encounters, the strong attractor sites are well distinguished, having detainment energies of $\Delta G_{\text{det}} \approx -k_{\text{B}}T$ or less, while the weaker attractor sites have $\Delta G_{\text{det}} > 0$. In the case of the sodium ions, all the attractor sites are of the same chemical nature and yet, there are marked differences between the detainment energies associated with the sites. Thus, the capacity of a site to detain an ion is not attributed to the residue itself. Rather, it is a reflection of multiple interactions of many moieties on the protein's surface. These interactions render, for example, the uncharged histidine residue His16 a stronger attractor than some of the glutamate and aspartate residues. Apparently, its location under the umbrella of the negative domain of the electrostatic field exerted by the protein (see Figure 4A below) increases its probability to interact with the Na^+ ion. In the case of chloride, three residues that are clustered together (Figure 6B below) form a strong attractor site where the Cl^- ions can be detained, hopping from one residue to another.

THE ELECTROSTATIC POTENTIAL AROUND THE PROTEIN

The apparent selectivity of the ion attractor sites suggests that the detainment is determined not by a single residue but rather by the electrostatic potential surrounding the protein, which is displayed in Figure 4. The potential field around the protein consists of two main lobes, one positive and the other negative. The ions are attracted to the oppositely charged lobes, and move preferentially back and forth within the boundary of the Coulomb cage of the protein, interacting with the residues enclosed within this space.

The negative Coulomb cage has a linear array of attractors; the Na^+ ions shuttle along this array. Figure 4A shows a time window where the preferential site for the Na^+ ion is next to the relatively weak attractor His16. During the simulation, the sodium ions spend more time near the two other attractors (namely Glu95 and Glu41) that are shown in Figure 4A.

To quantitate the passage of the ion between the sites we used, a binary function that has the value of 1 if the ion is detained by a certain site and otherwise a value of 0. Figure 5A represents the passage of a single Na^+ ion during the first 1.5 nanosecond of the simulation time. Between 200 and 800 picoseconds of simulation time, the sodium ion undergoes a series of encounters with Glu95. It then briefly visits Glu41

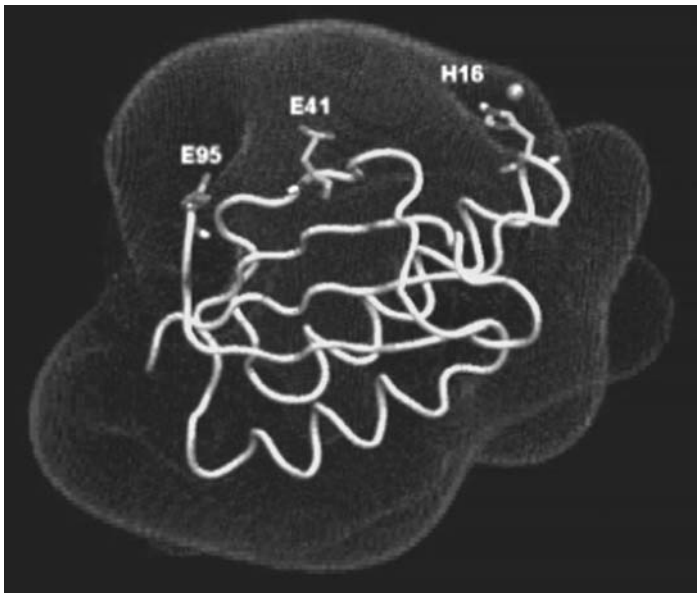

(A)

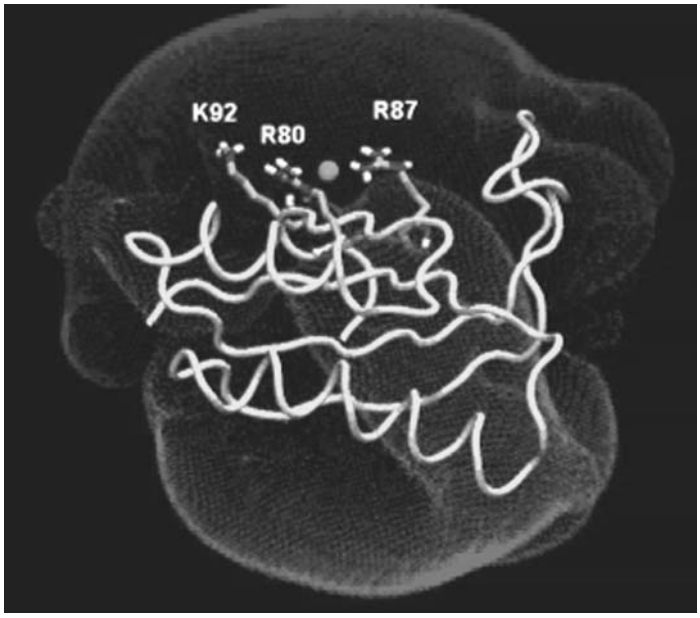

(B)

Figure 4. The electrostatic potential surface around the protein. (A) Residue His16 (which is transiently located in the vicinity of the ion) and the two attractor sites Glu41 and Glu95. (B) Residues Arg80 and Arg87, which are the strongest ion attractors, and Lys92, which is located in their vicinity and forms a weak ion attractor, are presented at the moment when the ion is detained by Arg80 and Arg87. The Coulomb cages for the positive (blue) and negative (red) domains are drawn at the distance where the electrostatic potential equals 1 k_BT/e.

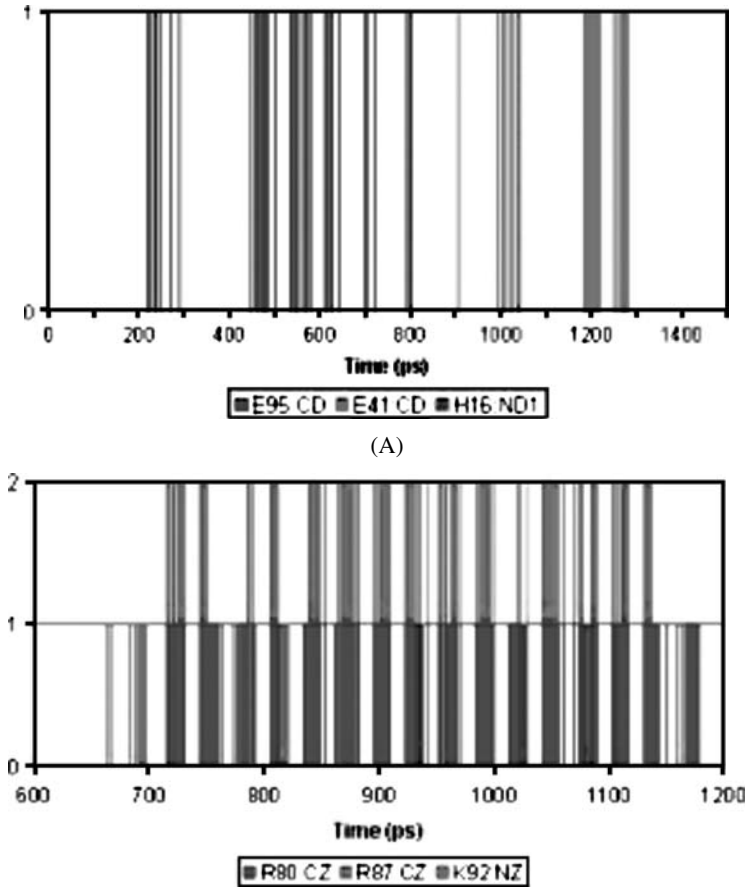

Figure 5. The number of contacts between ions and selected residues during the simulation. In the definition of contact, we use a function which is equal to 1 if the distance between the atom and the ion is smaller than 6 Å and equal to 0 otherwise. (A) The contact function calculated for one of the Na^+ ions and the attractor sites Glu95:CD (blue), Glu41:CD (red) or His16:ND1 (green) displayed as a function of simulation time. (B) The contact function calculated for one of the Cl^- ions and the attractor sites Arg80:CZ (green), Arg87:CZ (blue) or Lys92:NZ (red) displayed as a function of simulation time.

before being detained by His16 and again by Glu41. At ∼1300 picoseconds, the ion is released to the bulk. The encounter of the sodium ion with the uncharged histidine residue is enhanced by its previous detainment by the stronger attractors on the protein surface. The ion is able to migrate between the attractor sites stretched along the negative umbrella, where it samples the environment of the various residues.

The positive Coulomb cage (Figure 4B) has one central attractor area made of two arginines (Arg80 and Arg87). A nearby lysine residue, Lys92, forms a weaker attractor (see Table II). As presented in Figure 5B, one of the Cl^- ions first

encounters Lys92 and then shuttles to the two arginines where it exercises repeated encounters with the two positive sites. Close examination of the random motion of the Cl^- in the site reveals repeated interactions between the anion and the OH moiety of tyrosine 50, making it an apparent attractor with a value of $K_{det} = -3.51$ KJ/mol (see Table I).

THE THERMODYNAMIC CONSTITUENT OF THE BINDING ENERGY

Hitherto, the energies associated with the detainment of the ions were calculated based on the analysis of the MD simulation. It would be of interest to test whether similar binding energies can also be obtained through structural thermodynamic formalism.

Following Froloff *et al.* [55] the binding free energy can be estimated in the form:

$$\Delta G_{det} = \Delta G_{el} + \Delta G_{np} + \Delta G_{strain} - T\Delta S_{mc} - T\Delta S_{sc} - T\Delta S_{t,r;res} - T\Delta S_{t;ion} \tag{4}$$

where ΔG_{el} is the electrostatic contribution to the detainment energy, ΔG_{np} is the non-polar contribution due to a change in the exposed surface area, ΔG_{strain} is the change in free energy due to local distortions in the protein and the ligand, $T\Delta S_{mc}$ accounts for the loss of backbone torsional freedom, $T\Delta S_{sc}$ accounts for the loss of side chain torsional freedom, and $T\Delta S_{t,r;res}$ and $T\Delta S_{t;ion}$ account for the loss of translational and rotational freedom of the binding residues and for the loss of the translational freedom of the ion upon its detainment. When calculating the binding of a small ion to a protein, ΔG_{strain} can be neglected. ΔG_{np} and $T\Delta S_{sc}$ are also negligible since the binding of a small ion hardly modulates the exposure of the binding residues to the solvent interface (for elaboration of these terms, see Froloff *et al.* [55]). The loss of backbone torsional freedom of the residues following the binding of the ions is also expected to be negligible, i.e. $T\Delta S_{sc} \sim 0$.

The value of $\Delta S_{t,r;res}$ depends on the thermal motion of the atoms, which is proportional to their root mean square fluctuations (RMSF). Comparison of the RMSF of the residues of the Cl^--detaining site during the time of detainment versus the RMSF of the same residues when the site is free, revealed no significant difference. Therefore, we assume that the binding of the ion hardly influences the rotational and translational freedom of the binding residues, i.e. $\Delta S_{t,r;res} \sim 0$.

Taking all the above into account, we can simplify Eq. (4) in the case of the binding of an ion to the protein surface, as:

$$\Delta G_b \approx \Delta G_{el} - T\,\Delta S_{t;ion} \tag{5}$$

The electrostatic contribution to the detainment energy was calculated for two conformations of the protein when the ion was detained, as shown in Figure 6. These

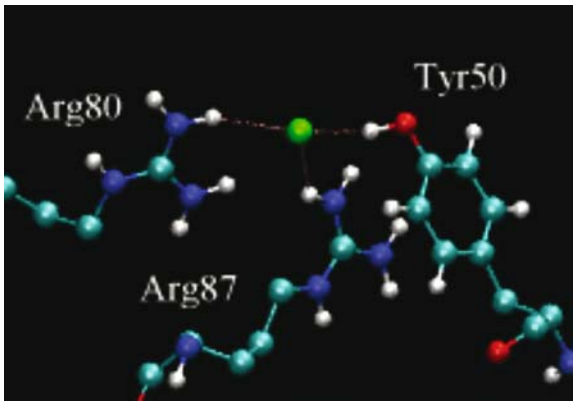

(A)

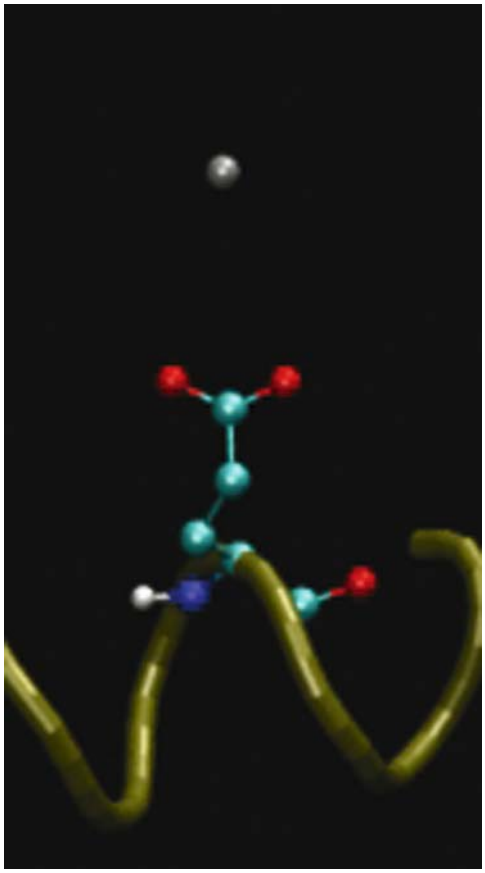

(B)

Figure 6. The bound ions and their immediate vicinity. (A) A chloride ion bound to residues Arg80, Arg87 and Tyr50. The minimal distances between the ion and the residues were 2.24 Å, 2.86 Å and 2.02 Å for Arg80, Arg87 and Tyr50, respectively. (B) A sodium ion bound to Glu31. The minimal distance between the ion and the protein is 4.34 Å.

Table III. The contributions for the free energies of detainment (see Eq. (5)).

	Na^+				Cl^-	
ε	ΔG_{el}	$T\Delta S_{t,ion}$	ΔG_b[(a)]	ΔG_b[(b)]	ΔG_{el}	ΔG_b[(b)]
4	−41.8	−10.3	−31.5	−2.3	−79.1	−3.8
10	−15.1	−10.3	−3.8	−2.3	−29.7	−3.8
20	−7.1	−10.3	+3.4	−2.3	−14.6	−3.8

Note. The energies are presented in KJ/mol. ε is the dielectric constant as used for the calculation of ΔG_{el} (see Methods).
[a]Calculated by Eq. (5).
[b]Reference energies, taken from Tables I and II, calculated throughout the 10 nanosecond simulation.

calculations are performed by solving the Poisson-Boltzmann equation, where the solutes are treated in atomic detail while the solvent is represented by a continuum. For these calculations, the dielectric constants of the solutes (protein and bound ions) and the solvent must be given as input. While the choice of a dielectric constant for the solvent is straightforward ($\varepsilon = 78.4$), the dielectric constant of a protein may assume different values, depending on the system under study. Miyashita and co-workers have calculated the binding energies for protein-protein association using different values of the solute's dielectric constant between $\varepsilon = 2$ and $\varepsilon = 20$ [56], finding reasonable agreement with the experiment when the dielectric constants of the proteins were $\varepsilon = 10$–20. Following their lead, we calculated the value of ΔG_{el} with the dielectric constant assigned for the solutes set as 4, 10 and 20. The corresponding values of ΔG_{el} are given in Table III.

While the electrostatic energy favors the detained state, the entropy term given in Eq. (5) favors the free state of the ion. Treating the ions in the bulk as ideal, non-interacting particles, the change of entropy upon the detainment of the ion can be estimated by:

$$\Delta S_{t,ion} = R \ln (V_d / V_f) \tag{6}$$

where V_d is the volume element available for the detained ion and V_f the volume available for the free ion. Following the operational definition of the detained state, the ion can be located within a range of 6 Å away from the nearest protein atom. Accordingly, we can estimate the free space sampled by the detained ion as the volume of a spheric shell having an outer radius of 0.6 nm and an inner radius which is determined by the Van der Waals exclusion distance around the ion (∼0.2 nm), i.e. $V_d = 0.87$ nm^3. When the ion is diluted in the bulk, the average volume that it occupies is a function of its concentration in the solution. For a solution of 0.03 M, $V_f = 55.37$ nm^3.

The entropic loss upon detainment of the free Na^+ ion ($T\Delta S_{t,Na^+}$) is calculated to be -10.29 KJ/mol. The calculation of $\Delta S_{t,Cl^-}$ is more complex, as the ion interacts with two bulky positive residues (Arg80 and Arg87) and, to a lesser extent, with the O–H dipole of Tyr50. Thus, the space it can sample while remaining within 6 Å of the nearest atom is much larger than the corresponding space for the sodium ion, i.e. $V_{d,Cl^-} > V_{d,Na^+}$, and the entropic contribution of the detainment of Cl^- will be smaller, i.e. $\Delta S_{t,Na^+} > \Delta S_{t,Cl^-}$. Thus, the special geometry of the Cl^- attractor domain allows it more freedom of motion. In parallel, the electrostatic attraction operating on the Cl^- is stronger than that affecting the Na^+ (Table III, column 6). The combination of the two factors leads to a higher detainment of the Cl^- with respect to the Na^+.

The energy associated with the detainment of the ions throughout the MD simulation (as calculated from Eq. (2)) is displayed in Table III as a reference value (columns 5 and 7 for the Na^+ and Cl^-, respectively). It can be observed that if the dielectric constant of the protein is set in the range of $10 \leq \varepsilon \leq 20$, the calculated detainment energy covers the range of its actual detainment energy. This range of dielectric constants assigned to the protein's surface is in accordance with Miyashita and co-workers [56].

Discussion

During the 10 nanosecond MD simulation of the Q16H/S17C S6 ribosomal protein mutant, which lacks any biological function associated with ion-binding, we could identify residues that function as local ion attractor sites. At these sites, the protein was able to confine ions to its immediate vicinity, 6 Å or less from its surface, for up to hundreds of picoseconds of simulation time. In the detained state, the ions did not lose their freedom of motion: they were able to shuttle between nearby attractor sites with a restriction that lowered their probability of moving far from the protein. This restriction is attributed to the electrostatic potential. As the ion could hop near an attractor site and between attractor sites in the detained state, even residues which are not expected to function as ion attractors (His 16 and Tyr 50) can draw the ions due to their location inside the Coulomb cage (Figure 4A) or near strong attractors (Figure 6A).

The simulation revealed fast exchange of the ions between the protein's surface and the bulk, reflecting a competition between two forces: the electrostatic attraction that favors the detainment and the entropic drive that prefers the free state of the ion. Therefore, throughout most of the simulation time, the ion diffuses in a Brownian motion in the bulk, but once an ion is trapped by the protein's Coulomb cage, it is drawn to the nearest attractor site. Sooner or later, depending on the strength of the attractor site, the ion will escape its detainment and will either diffuse within the Coulomb cage to another attractor or out of the Coulomb cage. Thus, an ion that is already located inside the Coulomb cage has a higher probability of encounter with other attractor sites. It should be mentioned that the interactions leading to the

detainment are rather weak, as the RMSF of the attractor residues is barely affected by the ion and the residues still execute their torsional and rotational motions.

There is a strong resemblance between the mechanism of ion motion next to the protein and the proton-collecting antenna reported for Bacteriorhodopsin [1, 24] or cytochrome c oxidase [57]. These domains consist of clusters of carboxylates that function as proton binding sites. The protonation on any carboxylate of the cluster leads to rapid proton exchange reactions that finally deliver the proton to the immediate vicinity of the proton-conducting channel of the protein.

In the present study, we generalized the system by substituting the proton, with its special chemistry, by more inert ions: Na^+ and Cl^-. Both bear one charge, yet they do not form a covalent bond with the protein and their diffusion mechanism is a simple self-diffusion rather than the Grotthuss mechanism of the proton [58]. With these ions we could follow the propagation along the surface of the protein without the complications emerging from the breaking of covalent bonds or the special diffusion pattern of the proton. The results clearly indicate that charged particles, once engaged in some interactions with the protein, will remain in its vicinity for a long time, thus increasing their probability of reacting with the nearby surface groups. For example, when a proton pumping protein (such as the bacteriorhodopsin or cytochrome oxidase) is fishing for a proton present at low concentration ($pH \geq 7$), there is a great advantage in forming a collecting antenna. The multiplicity of proton binding sites increases the probability that at a given time one of the proton binding sites will be protonated, and once one had reacted, the fast exchange will shuttle it to the moiety associated with the catalysis.

Acknowledgments

This research is supported by the Israel Science Foundation (grant No 427/01-1) and the United States-Israel Bi-National Science Foundation (grant No 2002129). R.F. acknowledges the Colton Foundation for its support through the Colton Scholarship. The authors would also like to acknowledge the use of computer resources belonging to the High Performance Computing Unit, a division of the Inter University Computing Center, which is a consortium formed by research universities in Israel. More information about this facility can be found at http://www.hpcu.ac.il.

References

1. Nachliel, E., Gutman, M., Tittor, J. and Oesterhelt, D.: Proton Transfer Dynamics on the Surface of the Late M State of Bacteriorhodopsin, *Biophys. J.* **83** (2002), 416–426.
2. Bizzarri, A.R. and Cannistraro, S.: Molecular Dynamics of Water at the Protein-Solvent Interface, *J. Phys. Chem. B* **106** (2002), 6617–6633.
3. Makarov, V., Pettitt, B.M. and Feig, M.: Solvation and Hydration of Proteins and Nucleic Acids: A Theoretical View of Simulation and Experiment, *Acc. Chem. Res*. **35** (2002), 376–384.

4. Svergun, D.I., Richard, S., Koch, M.H., Sayers, Z., Kuprin, S. and Zaccai, G.: Protein Hydration in Solution: Experimental Observation by X-ray and Neutron Scattering, *Proc. Natl. Acad. Sci. U.S.A.* **95** (1998), 2267–2272.
5. Smith, J.C., Merzel, F., Verma, C.S. and Fischer, S.: Protein Hydration Water: Structure and Thermodynamics, *J. Mol. Liquid* **101** (2002), 27–33.
6. Schiffer, C.A. and van Gunsteren, W.F.: Accessibility and Order of Water Sites in and Around Proteins: A Crystallographic Time-Averaging Study, *Proteins* **36** (1999), 501–511.
7. Sanschagrin, P.C. and Kuhn, L.A.: Cluster Analysis of Consensus Water Sites in Thrombin and Trypsin Shows Conservation Between Serine Proteases and Contributions to Ligand Specificity, *Protein Sci.* **7** (1998), 2054–2064.
8. Fenimore, P.W., Frauenfelder, H., McMahon, B.H. and Parak, F.G.: Slaving: Solvent Fluctuations Dominate Protein Dynamics and Functions, *Proc. Natl. Acad. Sci. U.S.A.* **99** (2002), 16047–16051.
9. Higo, J. and Nakasako, M.: Hydration Structure of Human Lysozyme Investigated by Molecular Dynamics Simulation and Cryogenic X-Ray Crystal Structure Analyses: On the Correlation Between Crystal Water Sites, Solvent Density, and Solvent Dipole, *J. Comput. Chem.* **23** (2002), 1323–1336.
10. Curtis, R.A., Prausnitz, J.M. and Blanch, H.W.: Protein-Protein and Protein-Salt Interactions in Aqueous Protein Solutions Containing Concentrated Electrolytes, *Biotechnol. Bioeng.* **57** (1998), 11–21.
11. Scheiner, S.: Quantum Chemical Studies of Proton Transport Through Biomembranes, *Ann. N.Y. Acad. Sci.* **367** (1981), 493–509.
12. Gutman, M., Huppert, D. and Nachliel, E.: Kinetic Studies of Proton Transfer in the Microenvironment of a Binding Site, *Eur. J. Biochem*. **121** (1982), 637–642.
13. Paddock, M.L., McPherson, P.H., Feher, G. and Okamura, M.Y.: Pathway of Proton Tranfer in Bacterial Reaction Centers: Replacement of Serinve-L22 by Alanine Inhibits Electron and Proton Transfers Associated with Reduction of Quinone to Dihydroquinone, *Proc. Natl. Acad. Sci. U.S.A.* **87** (1990), 6803–6807.
14. Bashford, D. and Gerwert, K.: Electrostatic Calculations of the pKa Values of Ionizable Groups in Bacteriorhodopsin, *J. Mol. Biol.* **224** (1992), 473–486.
15. Heberle, J., Riesle, J., Thiedemann, G., Oesterhelt, D. and Dencher, N.A.: Proton Migration Along the Membrane Surface and Retarded Surface to Bulk Transfer, *Nature* **370** (1994), 379–382.
16. McPherson, P.H., Schonfeld, M., Paddock, M.L., Okamura, M.Y. and Feher, G.: Protonation and Free Energy Changes Associated with Formation of QBH2 in Native and Glu-L212→Gln Mutant Reaction Centers from Rhodobacter Sphaeroides, *Biochemistry* **33** (1994), 1181–1193.
17. le Coutre, J. and Gerwert, K.: Kinetic Isotope Effects Reveal an Ice-Like and a Liquid-Phase-type Intramolecular Proton Transfer in Bacteriorhodopsin, *FEBS Lett*. **398** (1996), 333–336.
18. Gutman, M. and Nachliel, E.: Time Resolved Dynamics of Proton Transfer in Proteinous Systems, *Annu. Rev. Phys. Chem.* **48** (1997), 329–356.
19. Adelroth, P., Paddock, M.L., Sagle, L.B., Feher, G. and Okamura, M.Y.: Identification of the Proton Pathway in Bacterial Reaction Centers: Both Protons Associated with Reduction of QB to QBH2 Share a Common Entry Point, *Proc. Natl. Acad. Sci. U.S.A.* **97** (2000), 13086–13091.
20. Zscherp, C., Schlesinger, R. and Heberle, J.: Time-Resolved FT-IR Spectroscopic Investigation of the pH-Dependent Proton Transfer Reactions in the E194Q Mutant of Bacteriorhodopsin, *Biochem. Biophys. Res. Commun.* **283** (2001), 57–63.
21. Gutman, M., Nachliel, E., Mezer, A. and Noivirt, O.: Gauging of Local Micro-Environment at Protein Water Interface by Time-Resolved Single-Proton Transfer Reactions, *Ann. Eur. Acad. Sci.* **1** (2003), 75–107.

22. Nachliel, E. and Gutman, M.: Kinetic Analysis of Proton Transfer Between Reactants Adsorbed to the Same Micelle. The Effect of Proximity on the Rate Constants, *Eur. J. Biochem.* **143** (1984), 83–88.
23. Gutman, M., Nachliel, E., Bamberg, E. and Christensen, B.: Time-Resolved Protonation Dynamics of a Black Lipid Membrane Monitored by Capacitative Currents, *Biochim. Biophys. Acta* **905** (1987), 390–398.
24. Checover, S., Marantz, Y., Nachliel, E., Gutman, M., Pfeiffer, M., Tittor, J., Oesterhelt, D. and Dencher, N.A.: Dynamics of the Proton Transfer Reaction on the Cytoplasmic Surface of Bacteriorhodopsin, *Biochemistry* **40** (2001), 4281–4292.
25. Tran-Thi, T.H., Gustavsson, T., Prayer, C., Pommeret, S. and Hynes, J.T.: Primary Ultrafast Events Preceding the Photoinduced Proton Transfer from Pyranine to Water, *Chem. Phys. Lett.* **329** (2000), 421–430.
26. Forster, T. and Volker, S.: Kinetics of Proton Transfer Reaction Involving Hydroxypyrene-Trisulfonate in Aqueous Solution by Nanosecond Laser Absorption Spectroscopy, *Chem. Phys. Lett.* **34** (1975), 1–5.
27. Weller, A.: Excited State Proton Transfer, *Prog. React. Kinet.* **1** (1961), 198–214.
28. Gutman, M. and Huppert, D.: Rapid pH and deltamuH+ Jump by Short Laser Pulse, *J. Biochem. Biophys. Methods* **1** (1979), 9–19.
29. Checover, S., Nachliel, E., Dencher, N.A. and Gutman, M.: Mechanism of Proton Entry into the Cytoplasmic Section of the Proton-Conducting Channel of Bacteriorhodopsin, *Biochemistry* **36** (1997), 13919–13928.
30. Marantz, Y., Nachliel, E., Aagaard, A., Brzezinski, P. and Gutman, M.: The Proton Collecting Function of the Inner Surface of Cytochrome C Oxidase from Rhodobacter Sphaeroides, *Proc. Natl. Acad. Sci. U.S.A.* **95** (1998), 8590–8595.
31. Cohen, B. and Huppert, D.: Evidence for a Continuous Transition from Nonadiabatic to Adiabatic Proton Transfer Dynamics in Protic Solvents. *J. Phys. Chem. A* **105** (2001), 2980–2988.
32. Agalarov, S.C., Prasad, G.S., Funke, P.M., Stout, C.D. and Williamson, J.R.: Structure of the S15,S6,S18-rRNA Complex: Assembly of the 30S Ribosome Central Domain, *Science* **288** (2000), 107–112.
33. Lindahl, E., Hess, B. and van der Spoel, D.: Gromacs 3.0: A Package for Molecular Simulation and Trajectory Analysis, *J. Mol. Med.* **7** (2001), 306–317.
34. van Gunsteren, W.F. and Berendsen, H.J.C.: *Gromos-87 Manual*, Biomos BV, Groningen, 1987.
35. van Buuren, A.R., Marrink, S.J. and Berendsen, H.J.C.: A Molecular Dynamics Study of the Decane/Water Interface, *J. Phys. Chem.* **97** (1993), 9206–9212.
36. Mark, A.E., van Helden, S.P., Smith, P.E., Janssen, L.H.M. and van Gunsteren, W.F.: Convergence Properties of Free Energy Calculations: Alpha-Cyclodextrin Complexes as a Case Study, *J. Am. Chem. Soc.* **116** (1994), 6293–6302.
37. van Buuren, A.R. and Berendsen, H.J.C.: Molecular Dynamics Simulations of the Stability of a 22 Residue Alpha-Helix in Water and 30% Trifluoroethanol, *Biopolymers* **33** (1993), 1159–1166.
38. Liu, H., Muller-Plathe, F. and van Gunsteren, W.F.A.: Force Field for Liquid Dimethyl Sulfoxide and Liquid Proporties of Liquid Dimethyl Sulfoxide Calculated Using Molecular Dynamics Simulation, *J. Am. Chem. Soc.* **117** (1995), 4363–4366.
39. Lindahl, M., Svensson, L.A., Liljas, A., Sedelnikova, S.E., Eliseikina, I.A., Fomenkova, N.P., Nevskaya, N., Nikonov, S.V., Garber, M.B. and Muranova, T.A.: Crystal Structure of the Ribosomal Protein S6 from Thermus Thermophilus, *EMBO J.* **13** (1994), 1249–1254.
40. Berman, H.M., Westbrook, J., Feng, Z., Gilliland, G., Bhat, T.N., Weissig, H., Shindyalov, I.N. and Bourne, P.E.: The Protein Data Bank, *Nucleic Acids Res.* **28** (2000), 235–242.
41. Berendsen, H.J.C., Postma, J.P.M., van Gunsteren, W.F. and Hermans, J.: Interaction Models for Water in Relation to Protein Hydration, *Nature* **224** (1969), 175–177.

42. van der Spoel, D. and Berendsen, H.J.C.: Molecular Dynamics Simulations of Leu-Enkephalin in Water and DMSO, *Biophys. J.* **72** (1997), 2032–2041.
43. Tieleman, D.P. and Berendsen, H.J.C.: Molecular Dynamics Simulations of a Fully Hydrated Dipalmitoylphosphatidylcholine Bilayer with Different Macroscopic Boundary Conditions and Parameters, *J. Chem. Phys.* **105** (1996), 4871–4880.
44. Hess, B., Bekker, H., Berendsen, H.J.C. and Fraaije, J.G.E.M.: LINCS: A Linear Constraint Solver for Molecular Simulations, *J. Comp. Chem.* **18** (1997), 1463–1472.
45. Miyamoto, S. and Kollman, P.A.: SETTLE: An Analytical Version of the SHAKE and RATTLE Algorithms for Rigid Water Models, *J. Comp. Chem.* **13** (1992), 952–962.
46. Berendsen, H.J.C., Postma, J.P.M., DiNola, A. and Haak, J.R.: Molecular Dynamics with Coupling to an External Bath, *J. Chem. Phys.* **81** (1984), 3684–3690.
47. Darden, T., York, D. and Pedersen, L.: Particle Mesh Ewald: An N-log(N) Method for Ewald Sums in Large Systems, *J. Chem. Phys.* **98** (1993), 10089–10092.
48. Baker, N.A., Sept, D., Joseph, S., Holst, M.J. and McCammon, J.A.: Electrostatics of Nanosystems: Application to Microtubules and the Ribosome, *Proc. Natl. Acad. Sci. U.S.A.* **98** (2001), 10037–10041.
49. Humphrey, W., Dalke, A. and Schulten, K.: VMD: Visual Molecular Dynamics, *J. Mol. Gr.* **14** (1996), 33–38.
50. van der Spoel, D., van Maaren, P.J. and Berendsen, H.J.C.: A Systematic Study of Water Models for Molecular Simulation: Derivation of Water Models Optimized for Use with a Reaction Field, *J. Chem. Phys.* **108** (1998), 10220–10230.
51. Harned, S.H. and Hildreth, C.L.: The Differential Diffusion Coefficients of Lithium and Sodium Chlorides in Dilute Aqueous Solution at 25 degrees. *J. Am. Chem. Soc.* **73** (1951), 650–652.
52. Stokes, R.H.: The Diffusion Coefficients of Eight Uni-Univalent Electrolytes in Aqueous Solution at 25, *J. Am. Chem. Soc.* **72** (1950), 2243–2247.
53. Macdonald, P.M. and Seelig, J.: Anion Binding to Neutral and Positively Charged Lipid Membranes, *Biochemistry* **27** (1988), 6769–6775.
54. Pandit, S.A., Bostic, D. and Berkowitz, M.L.: Molecular Dynamics Simulation of a Dipalmitoylphosphatidylcholine Bilayer with NaCl, *Biophys. J.* **84** (2003), 3743–3750.
55. Froloff, N., Windemuth, A. and Honig, B.: On the Calculation of Binding Free Energies Using Continuum Methods: Application to MHC Class I Protein-Peptide Interactions, *Protein Sci.* **6** (1997), 1293–1301.
56. Miyashita, O., Onuchic, J.N. and Okamura, M.Y.: Continuum Electrostatic Model for the Binding of Cytochrome c2 to the Photosynthesis Reaction Center from Rhodobacter Sphaeroides, *Biochemistry* **42** (2003), 11651–11660.
57. Marantz, Y., Einarsdottir, O.O., Nachliel, E. and Gutman, M.: Proton-Collecting Properties of Bovine Heart Cytochrome C Oxidase: Kinetic and Electrostatic Analysis, *Biochemistry* **40** (2001), 15086–15097.
58. Agmon, N.: The Grotthuss Mechanism, *Chem. Phys. Lett.* **244** (1995), 456–462.